Discovery of a Be/X-ray pulsar binary and associated supernova remnant in the Wing of the Small Magellanic Cloud

V. Hénault-Brunet,[1]⋆ L. M. Oskinova,[2] M. A. Guerrero,[3] W. Sun,[4] Y.-H. Chu,[5]
C. J. Evans,[1,6] J. S. Gallagher III,[7] R. A. Gruendl[5] and J. Reyes-Iturbide[8]

[1]*Scottish Universities Physics Alliance (SUPA), Institute for Astronomy, University of Edinburgh, Blackford Hill, Edinburgh EH9 3HJ*
[2]*Institute for Physics and Astronomy, University of Potsdam, 14476 Potsdam, Germany*
[3]*Instituto de Astrofísica de Andalucía, IAA-CSIC, Glorieta de la Astronomía s/n, 18008 Granada, Spain*
[4]*Department of Astronomy, Nanjing University, Nanjing, 210093 Jiangsu, China*
[5]*Department of Astronomy, University of Illinois, 1002 West Green Street, Urbana, IL 61801, USA*
[6]*UK Astronomy Technology Centre, Royal Observatory Edinburgh, Blackford Hill, Edinburgh EH9 3HJ*
[7]*Department of Astronomy, University of Wisconsin-Madison, 5534 Sterling, 475 North Charter Street, Madison, WI 53706, USA*
[8]*Escuela Superior de Física y Matemáticas, IPN, U.P. Adolfo López Mateos, C.P. 07738 D.F., Mexico*

ABSTRACT

We report on a new Be/X-ray pulsar binary located in the Wing of the Small Magellanic Cloud (SMC). The strong pulsed X-ray source was discovered with the *Chandra* and *XMM–Newton* X-ray observatories. The X-ray pulse period of 1062 s is consistently determined from both *Chandra* and *XMM–Newton* observations, revealing one of the slowest rotating X-ray pulsars known in the SMC. The optical counterpart of the X-ray source is the emission-line star 2dFS 3831. Its B0-0.5(III)e+ spectral type is determined from VLT-FLAMES and 2dF optical spectroscopy, establishing the system as a Be/X-ray binary (Be-XRB). The hard X-ray spectrum is well fitted by a power law with additional thermal and blackbody components, the latter reminiscent of persistent Be-XRBs. This system is the first evidence of a recent supernova in the low-density surroundings of NGC 602. We detect a shell nebula around 2dFS 3831 in Hα and [O III] images and conclude that it is most likely a supernova remnant. If it is linked to the supernova explosion that created this new X-ray pulsar, its kinematic age of $(2–4) \times 10^4$ yr provides a constraint on the age of the pulsar.

Key words: stars: emission-line, Be – ISM: supernova remnants – Magellanic Clouds – X-rays: binaries.

1 INTRODUCTION

The Small Magellanic Cloud (SMC) is host to a large population of ∼50 high-mass X-ray binaries (HMXBs), comparable to the number known in the Galaxy (e.g. Haberl & Pietsch 2004; Coe et al. 2005; Reig 2011). However, unlike the Galactic population, all of these systems but one are Be/X-ray binary (Be-XRB) systems, with the exception (SMC-X1) containing a supergiant companion instead (Webster et al. 1972).

The Wing of the SMC is the region linking the eastern side of the SMC to the Bridge. Despite its lower content of gas, dust and stars, it had a major star-forming event ∼11 Myr ago and appears, as expected, deficient in Be-XRBs (Antoniou et al. 2010). Note, however, that the coverage of the SMC Wing by X-ray observations has been sparser than that of the Bar. Each new discovery of a Be-

XRB in the SMC Wing is therefore particularly noteworthy (e.g. McGowan et al. 2007).

We have conducted *Chandra* and *XMM–Newton* observations of the far eastern region of the Wing, concentrating on the star-forming region NGC 602. The full description of these observations will be presented in a forthcoming paper (Oskinova et al., in preparation). In this Letter, we concentrate on one bright X-ray source located near NGC 602 in projection and coinciding with the emission-line star 2dFS 3831 (RA = 1ʰ27ᵐ46ˢ03, Dec. = −73°32′56″42, J2000.0), which is revealed as a Be-XRB. Based on the results of Section 2.2, throughout this Letter we will refer to the X-ray source as SXP 1062 following the nomenclature of Coe et al. (2005) for SMC X-ray pulsars.

The stellar population of NGC 602 (which comprises three star clusters: NGC 602 A, B and C) has been studied in detail. In addition to very old stars of 6–8 Gyr, likely the SMC field population, the NGC 602 clusters contain young stars of ∼4–5 Myr (Westerlund 1964; Hutchings, Cartledge & Pazder 1991; Cignoni et al. 2009). The significant number of young stellar objects detected in

⋆E-mail: vhb@roe.ac.uk

the NGC 602A cluster (Carlson et al. 2007; Gouliermis, Quanz & Henning 2007) suggests that star formation is still ongoing. As for what initially triggered the formation of these clusters, the low-density environment in the Wing of the SMC hints at an additional mechanism acting along with gravitational collapse. NGC 602 is located at the intersection of three H I shells, and Nigra et al. (2008) suggested that its formation is the result of the interaction of two expanding shells ∼7 Myr ago. Schmalzl et al. (2008) proposed instead that star formation was possibly induced by encounters with the Large Magellanic Cloud or the Milky Way. NGC 602 is associated with SGS-SMC1, the only Hα supergiant shell known in the SMC. The discovery of a Be-XRB in this area (only ∼7 arcmin to the west of NGC 602A) provides important clues to the star formation history in the Wing and the evolution of large-scale structures in the interstellar medium.

This Letter is organized as follows. We describe the X-ray observations and analysis in Section 2. In Section 3, we present the spectroscopy of the optical counterpart. We discuss the properties and environment of SXP 1062 in Section 4 and present our conclusions in Section 5.

2 X-RAY OBSERVATIONS

The X-ray data were obtained with the ACIS-I camera on the *Chandra X-ray Observatory* and with the EPIC cameras onboard *XMM–Newton*. The *Chandra* observations consisted of 11 separate exposures acquired between 2010 March 31 and 2010 April 29 (effective exposure time of 290.7 ks), while four separate exposures were obtained with *XMM–Newton* between 2010 March 25 and 2010 April 12 (EPIC-pn effective exposure time of 162.5 ks). The data were reduced using the most up-to-date versions of the corresponding data reduction software. The X-ray source CXO J012745.97−733256.5 (= SXP 1062) coinciding with the optical emission-line star 2dFS 3831 is detected in each of these 15 exposures. In the *Chandra* observations, the positional uncertainty (1σ) of the X-ray source is 0.9 arcsec. The average background-subtracted count rates are 0.0548 ± 0.0004 and 0.1227 ± 0.0019 count s^{-1} respectively for the *Chandra* pointings in the 0.5–10.0 keV band and the *XMM–Newton* EPIC-pn observations in the 0.2–12.0 keV band. The source was also detected during an *XMM–Newton* slew on 2009 November 16. Interestingly, the source was not detected in the *ROSAT* All Sky Survey, although at its present luminosity it would have been bright enough at an expected *ROSAT* PSPC count rate of 0.01 count s^{-1}.

2.1 Spectral analysis

Fig. 1 shows the combined background-subtracted *Chandra* and *XMM–Newton* spectra of SXP 1062. The *Chandra* spectra were extracted from a 12.8-arcsec circular region and the background was extracted from a concentric annular region of radii 12.8 and 19.2 arcsec which was free of sources. Likewise, the *XMM–Newton* spectra were extracted from a 32-arcsec circular region and the background from four adjacent circular regions free of sources with radius 45 arcsec.

As a first step, the background-subtracted *Chandra* and *XMM–Newton* spectra of SXP 1062 were simultaneously fitted using a simple absorbed power-law model. The best-fitting parameters, listed in Table 1, imply an absorbed flux in the energy range 0.2–12.0 keV of $f_X = 1.8 \times 10^{-12}$ erg cm^{-2} s^{-1}. This corresponds to an intrinsic X-ray luminosity in this same energy range of $L_X = 6.9 \times 10^{35}$ erg s^{-1} assuming a distance modulus of 18.7 appropriate for the Wing (e.g.
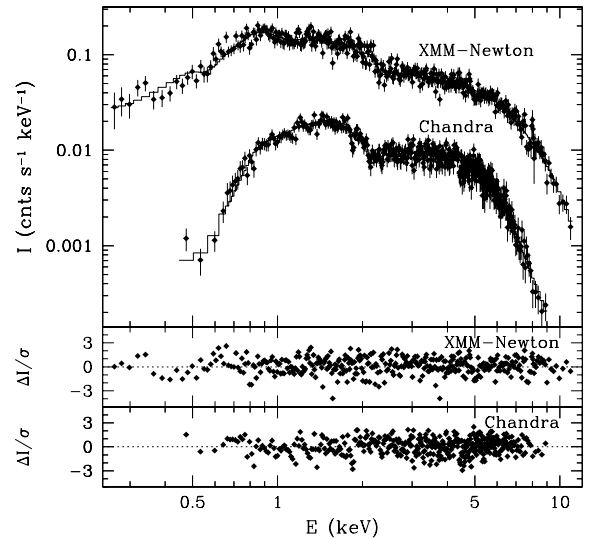

Figure 1. *Chandra* ACIS-I and *XMM–Newton* EPIC-pn spectra of SXP 1062. Overplotted is the best-fitting model including power-law, thermal and blackbody components. The lower panels show the residuals of the fit.

Cignoni et al. 2009), or $L_X = 8.2 \times 10^{35}$ erg s^{-1} for the 'standard' SMC distance modulus of 18.9 (e.g. Harries et al. 2003). The photon index Γ of ∼0.75 is typical of X-ray pulsar binaries (e.g. Yokogawa et al. 2003) and a signature of accretion onto a strongly magnetized neutron star.

The simple power-law model suggests some emission excess below 1 keV and at high energies. As a next step, we added a blackbody component, which statistically improved the fit (see Table 1). The observed X-ray flux is similar to that of the previous model, but the X-ray luminosity decreases by ∼10 per cent. We also tried a model for which a thermal plasma component with SMC abundances is included instead of a blackbody. Similarly to the blackbody, the addition of a thermal component to the power-law model improves the fit. In this case, the intrinsic X-ray luminosity is only marginally greater by ∼1 per cent compared to the simple power-law model.

Finally, the best fit is achieved by adding simultaneously a thermal and a blackbody component to the power law (see Table 1 and Fig. 1). The flux for this model (PBT in Table 1) is $f_X = 1.66^{+0.19}_{-0.25} \times 10^{-12}$ erg cm^{-2} s^{-1}, corresponding to an intrinsic luminosity $L_X = 6.3^{+0.7}_{-0.8} \times 10^{35}$ erg s^{-1} for a distance modulus of 18.7.

The column densities are well constrained by spectral fitting, albeit the values slightly differ depending on the model. Using the best-fitting values, we note that the H column densities in Table 1 imply $A_V = 0.63$–0.87 mag for the N_H/A_V ratio of 1.87×10^{21} cm^{-2}, i.e. $E(B - V) = 0.20$–0.28 assuming $R_V = 3.1$. This range is in good agreement with the $E(B - V) = 0.19$ value computed by comparing the value $(B - V) = -0.04$ of 2dFS 3831 (Massey 2002) with the intrinsic value $(B - V)_0 = -0.23$ of a B0-0.5III star (Wegner 1994) given the uncertainties on the photometry and spectral type (see Section 3 for the optical spectroscopy of 2dFS 3831).

2.2 Timing analysis

The photon arrival times were corrected for the Solar system barycentre. We searched for pulsations in the X-ray light curves in the soft and hard energy bands (0.4–1.5, 2.0–7.2 keV) and a total energy band (0.4–7.2 keV), using fast Fourier transform and light-curve folding techniques as implemented in the timing analysis

Table 1. Best-fitting parameters of the spectral models. The codes for the different components of each model are 'P' for power law, 'B' for blackbody and 'T' for optically thin thermal emission with SMC abundances.

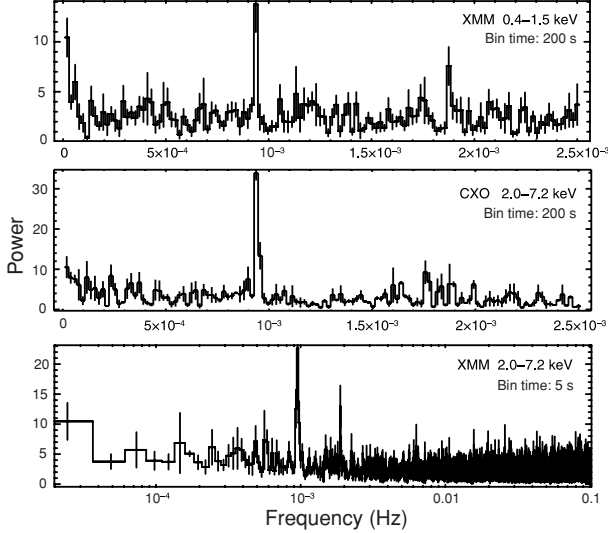| Model	N_H $(10^{21}$ cm$^{-2})$	Γ	$A_{power\ law}$ (phot keV^{-1} cm^{-2} s^{-1})	kT (keV)	$A_{blackbody}$ $(10^{39}$ erg s^{-1} kpc$^{-2})$	kT (keV)	$A_{thermal}$ $(10^9$ cm$^{-5})$	χ^2/d.o.f.
P	1.18 ± 0.06	0.746 ± 0.011	$(6.60 \pm 0.11) \times 10^{-5}$	–	–	–	–	1.30
PB	1.48 ± 0.12	1.185 ± 0.022	$(6.35 \pm 0.35) \times 10^{-5}$	2.13 ± 0.05	$(1.11 \pm 0.20) \times 10^{-5}$	–	–	1.21
PT	1.63 ± 0.04	0.732 ± 0.011	$(6.48 \pm 0.12) \times 10^{-5}$	–	–	0.589 ± 0.032	2.60 ± 0.32	1.19
PBT	1.35 ± 0.12	0.767 ± 0.027	$(4.87 \pm 0.30) \times 10^{-5}$	1.54 ± 0.16	$(4.5 \pm 0.9) \times 10^{-6}$	0.648 ± 0.029	2.80 ± 0.30	1.07

Figure 2. *XMM–Newton* and *Chandra* power density spectra in the soft and hard energy bands for different bin times.
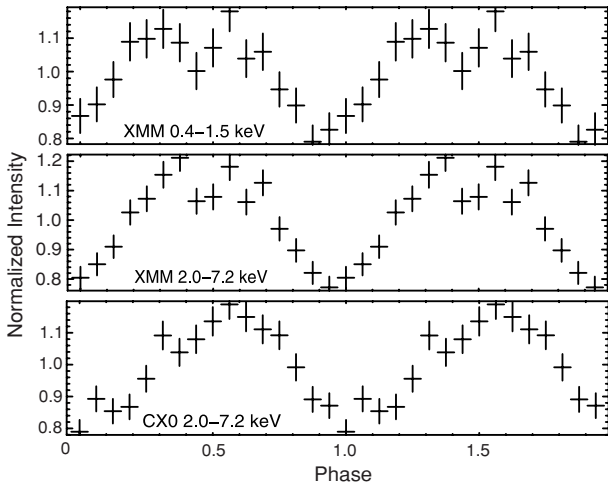

Figure 3. Pulse profiles folded with a period of 1062 s in different energy bands.

software XRONOS. Fig. 2 shows the inferred *Chandra* and *XMM–Newton* power density spectra in the soft and hard energy bands with a clear peak at a frequency of 9.4×10^{-4} Hz ($P = 1062$ s). This coherent X-ray pulse period establishes the source as a binary X-ray pulsar. The pulse profiles folded with this period are shown in Fig. 3.

The light curves used to compute the *XMM–Newton* power spectrum in the hard energy band, the *XMM–Newton* power spectrum in the soft energy band and the *Chandra* power spectrum in the

hard energy band were binned by 5, 200 and 200 s, respectively. The 5 s bin time for one of these was chosen to make sure that a shorter pulse was not missed. No pulse was found in the soft band *Chandra* observations, possibly because the count rate is too low. Because of the softer response of the EPIC-pn camera, the pulse in the soft band is the most obvious in the light curves obtained with this instrument.

Note that in addition to the pulse period, X-ray variability was also detected at a level of ∼20 per cent peak-to-peak on a time-scale of several days in both *XMM–Newton* and *Chandra* light curves. Given that this variability does not appear regular and that the time sampling is very sparse, we do not analyse these variations further.

3 OPTICAL SPECTROSCOPY

From its X-ray position with subarcsecond precision from *Chandra* images, the optical counterpart to SXP 1062 is identified as 2dFS 3831 (Evans et al. 2004). We observed this star with the VLT-FLAMES instrument (Pasquini et al. 2002) on 2010 October 25 as part of a spectroscopic survey of massive stars in NGC 602 complementing our X-ray observations. Spectra were obtained in the Medusa-fibre mode of FLAMES using the LR02 setting of the Giraffe spectrograph (3960–4564 Å, $R = 7000$, e.g. Evans et al. 2011). Five pairs of 1800-s exposures were obtained. The standard data processing (bias subtraction, fibre location, summed extractions, division by flat-field, wavelength calibration) was done using the ESO Common Pipeline Library FLAMES reduction routines (v.2.8.7). Additionally, heliocentric correction and subtraction of a median sky spectrum were performed (for details, see e.g. Evans et al. 2011). The spectra from all the exposures were then normalized and merged. The 2dF spectra of this star were also retrieved. These two spectra cover the regions from ∼3800 to 4900 Å and ∼6000 to 7000 Å, with resolving powers of 1500 and 2500, respectively (Evans et al. 2004). Fig. 4 shows the VLT-FLAMES and 2dF spectra of 2dFS 3831. The VLT-FLAMES spectrum has been smoothed and rebinned to an equivalent resolving power of $R = 4000$.

A weak He II λ4542 absorption line is visible in the VLT-FLAMES spectrum and there is a hint of a weak He II λ4686 line in the 2dF spectrum, but He II λ4200 is absent, suggesting a spectral type around B0-0.5 following the classification adopted by Evans et al. (2004).

Several characteristics attributable to a circumstellar disc indicate that 2dFS 3831 is a classical Be star. Fe II λ4179 and Fe II λ4233 emission lines typical of some early Be stars (e.g. Slettebak 1982) are visible in the VLT-FLAMES spectrum. The Hα emission seen in the 2dF spectrum (see the right-hand panel in Fig. 4) is relatively strong with an equivalent width (EW) of −23 Å. There is significant Hβ emission, plus emission in the core of the other Balmer lines (double-peaked in the VLT-FLAMES spectrum) and apparent infilling of the He I absorption lines. Two Micron All Sky Survey
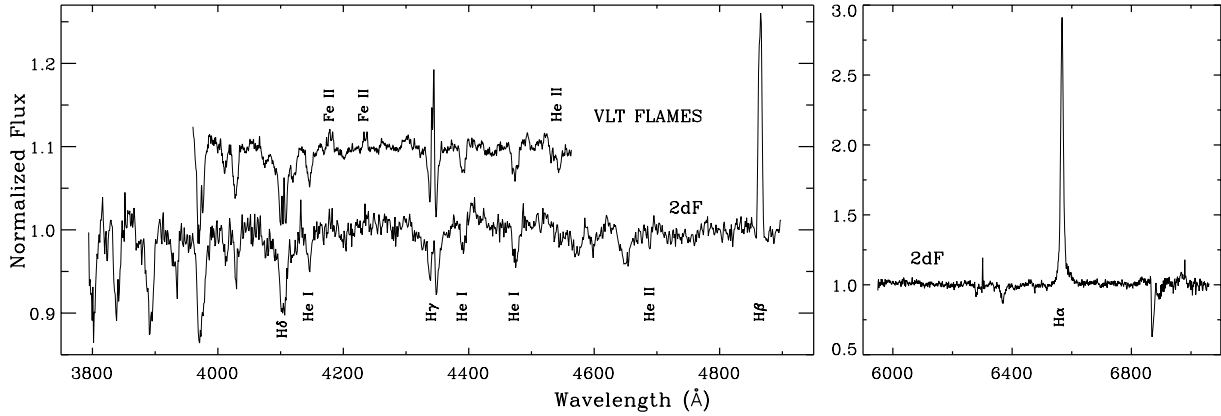
Figure 4. Optical VLT-FLAMES and 2dF spectra of 2dFS 3831 with key spectral features identified. The VLT-FLAMES spectrum is offset vertically.

(2MASS; Skrutskie et al. 2006) JHK_s photometry also indicates a clear infrared excess when compared with expected colours for a B0-0.5 spectral type (Wegner 1994). The double-peaked emission in the Balmer lines is not due to oversubtraction of nebular features present in the median sky spectrum. Also, given the relative weakness of the nebular emission lines in the mean sky spectrum, the emission in the core of the Balmer lines is most likely dominated by circumstellar material and not by nebular contamination.

The observed magnitude ($V = 14.36, B = 14.32$; Massey 2002) and a range of reasonable extinction estimates (including both the interstellar and circumstellar components) lead to an absolute magnitude consistent with a B0-0.5 giant (Walborn 1972; Vacca, Garmany & Shull 1996). We thus determine the spectral type of 2dFS 3831 as B0-0.5(III)e+, where '+' signifies the presence of Fe II. This corresponds to a typical effective temperature $T_{eff} \sim 26\,000$ K and an evolutionary mass $M \sim 15\,M_\odot$ at SMC metallicity (cf. Trundle et al. 2007).

We estimated the radial velocity of 2dFS 3831 from the VLT-FLAMES spectrum by fitting Gaussian profiles to the wings of Hγ, Hδ, Hϵ, He I λ4143 and He I λ4388. The average of all measurements is 167 kms^{-1} with a standard deviation of 13 kms^{-1}. This is consistent with the mean velocity of massive stars in the SMC (Evans & Howarth 2008), and also with the gas velocities measured by Nigra et al. (2008) across the N 90 H II region ionized by NGC 602A. Thus, we do not see any evidence that the HMXB acquired a high space velocity following the supernova explosion.

4 DISCUSSION

4.1 The properties of SXP 1062

SXP 1062 is only the third SMC X-ray pulsar with a spin period larger than 1000 s (Laycock et al. 2010). These slowly rotating pulsars are particularly interesting because they represent a challenge for the theory of spin evolution of a neutron star in a close binary system (e.g. Ikhsanov 2007).

According to the Corbet diagram for SMC Be-XRBs relating spin and orbital period (Corbet et al. 2009), we expect SXP 1062 to have a binary period of $\sim$300 d. Such a long orbital period is also expected from the P_{orb}–EW(Hα) diagram (Reig, Fabregat & Coe 1997), from which our measured EW(Hα) suggests an orbital period of $\sim$100 d. Note however that the maximum EW(Hα) of the system, which probes the maximum size of the disc (and indirectly the orbital

period), could be higher than our instantaneous measurement, so this period estimate should be taken as a lower limit.

SXP 1062 shares many characteristics with the class of persistent Be-XRBs (e.g. Reig 2011): a relatively low X-ray luminosity $\sim$10^{34}–10^{35} erg s^{-1}, a slowly rotating pulsar with $P > 200$ s, a relatively flat light curve with sporadic and unpredicted increases in intensity by less than an order of magnitude, and a lack of iron lines at $\sim$6.4 keV indicative of small amounts of material in the vicinity of the neutron star. A thermal excess of blackbody type, with a high temperature ($kT > 1$ keV) and a small emission area ($R < 0.5$ km, consistent with a hotspot at the polar cap of the neutron star) has recently been suggested as a common feature of persistent Be-XRBs (La Palombara et al. 2009). Such a component is also identified in the X-ray spectrum of SXP 1062, for which we infer a size of $\sim$0.4 km for the blackbody source from our best-fitting models (Section 2.1).

4.2 The environment of SXP 1062

We detected a shell nebula around SXP 1062 in the Magellanic Cloud Emission-line Survey (MCELS; Smith et al. 1999) Hα image and in the higher resolution CTIO 4-m MOSAIC (Muller et al. 1998) Hα image (see Fig. 5). This shell is also detected in the MCELS [O III] image, but hardly in [S II]. We adopt below a distance modulus of 18.7. The shell is not uniform, with radii varying from 75 arcsec at the sharp rim on the north-east to 94 arcsec at the diffuse edge on the south-west. The peak surface brightness of the north-east rim is $\sim$6 $\times$ 10^{-17} erg cm^{-2} s^{-1} arcsec^{-2}, corresponding to an emission measure of 30 cm^{-6} pc. The width of the rim suggests that the shell thickness (ΔR) is 5–10 per cent of the shell radius (R). The longest emitting length at the shell rim is $2R[1 - (\Delta R/R)^2]^{1/2}$; thus, the rms density in the shell is 1.3 ± 0.3 H-atom cm^{-3}. The gas mass in the shell is $250 \pm 100\,M_\odot$. This large mass indicates that the shell gas must be dominated by interstellar material.

The shell morphology resembles supernova remnants (SNRs) in the Magellanic Clouds. The X-ray images also suggest that diffuse X-ray emission possibly associated with a SNR may be present in the vicinity of SXP 1062 (Oskinova et al., in preparation). As the shell mass is much larger than the typical supernova ejecta mass, we assume that the shell is a SNR in the Sedov phase. The kinetic energy in the shell would be $\sim$30 per cent of the supernova explosion energy. Adopting a canonical explosion energy of 10^{51} erg, the current shell kinetic energy is 3 $\times$ 10^{50} erg, and implies a shell expansion velocity of 350 ± 100 km s^{-1} and an age of
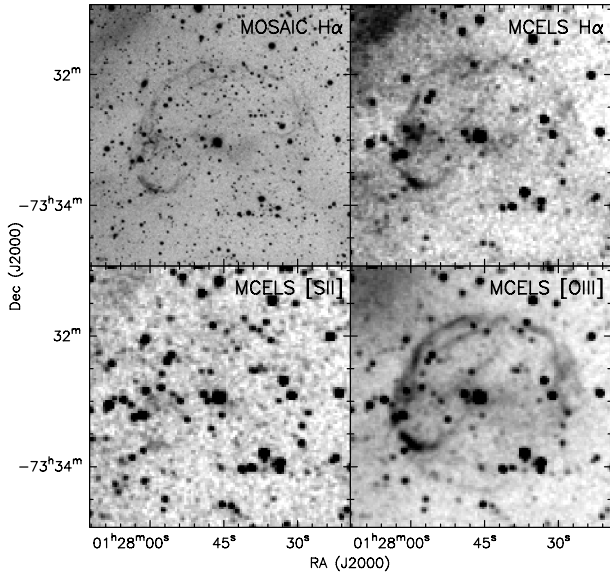
Figure 5. MOSAIC Hα image and MCELS Hα, [S II] and [O III] images of a region centred on the position of 2dFS 3831 = SXP 1062 and showing the shell nebula detected around the target.

$0.4(R/V) = (2–4) \times 10^4$ yr. This age is much larger than the cooling time-scale of this low-density gas, justifying an adiabatic shock for the Sedov phase. The pre-shock interstellar gas density, 1/4 the shell density, is 0.3 ± 0.1 H-atom cm^{-3}, consistent with the low density expected in the SMC Wing. The bright [O III] emission can be easily produced by a 350 km s^{-1} shock (cf. Hartigan, Raymond & Hartmann 1987). The ionizing flux of the B0-0.5III star can easily photoionize the shell gas and its surrounding pre-shock medium; furthermore, the diffuse [O III] emission to the north-east exterior of the shell indicates the existence of a harsh radiation field; therefore, the ionization stage of the pre-shock medium may be too high to produce strong post-shock [S II] emission. We thus conclude that the shell nebula detected around SXP 1062 is most likely a SNR. The extent of the shell, which has not reached the NGC 602 region, and its young kinematic age suggest that this supernova event did not trigger the formation of NGC 602.

5 CONCLUSION

We reported the discovery of a Be-XRB, SXP 1062, containing one of the slowest rotating X-ray pulsars in the SMC. We suggest that the shell nebula detected around this object is a SNR. Its estimated kinematic age of $(2–4) \times 10^4$ yr is probably the age of the pulsar. This is, to our knowledge, the first discovery of a pulsar associated with a SNR in the SMC.

ACKNOWLEDGMENTS

REFERENCES

Antoniou V., Zezas A., Hatzidimitriou D., Kalogera V., 2010, ApJS, 716, L140
Carlson L. R. et al., 2007, ApJS, 665, L109
Cignoni M. et al., 2009, AJ, 137, 3668
Coe M. J., Edge W. R. T., Galache J. L., McBride V. A., 2005, MNRAS, 356, 502
Corbet R. H. D., Coe M. J., McGowan K. E., Schurch M. P. E., Townsend L. J., Galache J. L., Marshall F. E., 2009, in van Loon J., Oliveira J. M., eds, Proc. IAU Symp. 256, The Magellanic System: Stars, Gas, and Galaxies. Kluwer, Dordrecht, p. 361
Evans C. J., Howarth I. D., 2008, MNRAS, 386, 826
Evans C. J., Howarth I. D., Irwin M. J., Burnley A. W., Harries T. J., 2004, MNRAS, 353, 601
Evans C. J., Taylor W. D., Hénault-Brunet V. et al., 2011, A&A, 530, A108
Gouliermis D. A., Quanz S. P., Henning T., 2007, ApJS, 665, 306
Haberl F., Pietsch W., 2004, A&A, 414, 667
Harries T. J., Hilditch R. W., Howarth I. D., 2003, MNRAS, 339, 157
Hartigan P., Raymond J., Hartmann L., 1987, ApJS, 316, 323
Hutchings J., Cartledge S., Pazder J., 1991, AJ, 101, 933
Ikhsanov N. R., 2007, MNRAS, 375, 698
La Palombara N., Sidoli L., Esposito P., Tiengo A., Mereghetti S., 2009, A&A, 505, 947
Laycock S., Zezas A., Hong J., Drake J. J., Antoniou V., 2010, ApJS, 716, 1217
McGowan K. E. et al., 2007, MNRAS, 376, 759
Massey P., 2002, ApJS, 141, 81
Muller G. P., Reed R., Armandroff T., Boroson T. A., Jacoby G. H., 1998, Proc. SPIE, 3355, 577
Nigra L., Gallagher J. S., Smith L. J., Stanimirović S., Nota A., Sabbi E., 2008, PASP, 120, 972
Pasquini L. et al., 2002, The Messenger, 110, 1
Reig P., 2011, Ap&SS, 332, 1
Reig P., Fabregat J., Coe M. J., 1997, A&A, 322, 193
Schmalzl M., Gouliermis D. A., Dolphin A. E., Henning T., 2008, ApJS, 681, 290
Skrutskie M. F. et al., 2006, AJ, 131, 1163
Slettebak A., 1982, ApJS, 50, 55
Smith R. C., The MCELS Team, 1999, in Chu Y. H., Suntzeff N., Hesser J., Bohlender D., eds, Proc. IAU Symp. 190, New Views of the Magellanic Clouds. Astron. Soc. Pac., San Francisco, p. 28
Trundle C., Dufton P. L., Hunter I., Evans C. J., Lennon D. J., Smartt S. J., Ryans R. S. I., 2007, A&A, 471, 625
Vacca W. D., Garmany C. D., Shull J. M., 1996, ApJS, 460, 914
Walborn N. R., 1972, AJ, 77, 312
Webster B. L., Martin W. L., Feast M. W., Andrews P. J., 1972, Nat, 240, 183
Wegner W., 1994, MNRAS, 270, 229
Westerlund B. E., 1964, MNRAS, 127, 429
Yokogawa J., Imanishi K., Tsujimoto M., Koyama K., Nishiuchi M., 2003, PASJ, 55, 161

This paper has been typeset from a TeX/LaTeX file prepared by the author.